



Enhanced Performance of Palladium Catalyst Confined Within Carbon Nanotubes for Heck Reaction

Zhengxiu Luo¹ · Deng Xiang¹ · Xiaoyan Pei¹ · Lu Wang² · Zhigang Zhao¹ · Wenjing Sun³ · Maofei Ran¹ · Tao Dai¹

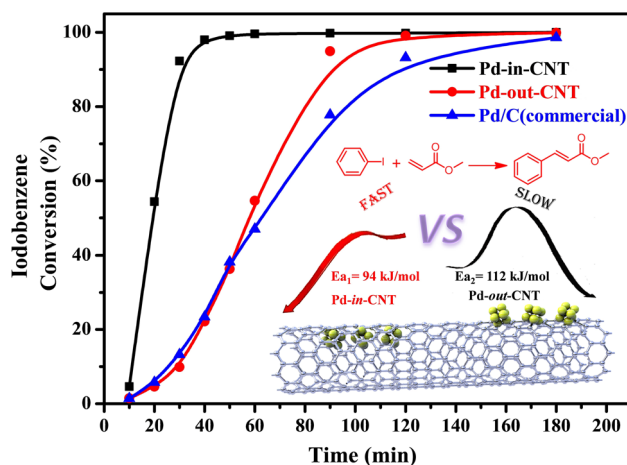
Received: 6 January 2021 / Accepted: 18 February 2021

© The Author(s), under exclusive licence to Springer Science+Business Media, LLC part of Springer Nature 2021

Abstract

Confined carbon nanotubes (CNTs) are typically used to tune the activity and stability of catalysts so as to increase their efficiency. Herein, we compared the catalytic performances of palladium nanoparticles (Pd NPs) located in different regions of CNTs for Heck reaction. The catalyst with Pd NPs located in the internal surface of CNTs (Pd-in-CNT) has a higher reaction rate than that with Pd NPs attached on the external surface of CNTs (Pd-out-CNT). The activity of the Pd-in-CNT is 9.4 times higher than that of Pd-out-CNT in the Heck reaction, possibly because of the smaller particle size and modified redox properties of the confined Pd NPs. The CNT cavities create more active sites, consistent with a higher microcalorimetric adsorption of carbon monoxide. Leaching of the Pd species during the reactions was observed with both types of catalysts. However, the Pd-in-CNT catalyst showed lower leaching than that of Pd-out-CNT owing to the spatial restriction of the channels in the former. More importantly, these novel catalysts were also used to synthesize a broad range of *p*-substituted iodobenzene derivatives, affording new and efficient route for the synthesis of valuable fine chemicals via carbon–carbon bond cross-coupling reactions.

Graphic Abstract



Keywords Heck reaction · Pd nanoparticles · Carbon nanotubes

1 Introduction

Traditional heterogeneous catalysts supported on carbon, metal oxides, and zeolites play an important role in synthetic methodology for the development of industrial processes, particularly in the production of fine chemicals [1–3].

✉ Maofei Ran
 Murphy_ran@foxmail.com

✉ Tao Dai
 tdaicat@163.com

Extended author information available on the last page of the article

The catalytic formation of carbon–carbon bonds via cross-coupling reactions has received much attention in organic chemistry [4–6], because it is one of the most useful tools for synthesizing natural products by linking two molecules. The Wurtz [7], Ullmann [8–10], Heck [11–13], Negishi [14], Stille [15], Suzuki [16, 17], and other such reactions [18, 19] are typical examples of cross-coupling reactions. Pd is the catalyst of choice for these reactions. Since 1972, various homogeneous catalysts based on Pd(0) and Pd(II) complexes with organic ligands have been developed [20], and many researchers including Ananikov [21], de Vries [22], and Schmidt [23] have detailed the mechanism of C–C bond formation with Pd metal catalysts. They have pointed out that the catalytic active centers of Pd may change dynamically.

For sustainable development, it is necessary to use reusable catalysts. Therefore, new catalytic systems should be developed to replace the existing homogeneous, non-reusable ones [24]. Recently, Pd-based heterogeneous catalysts have attracted significant attention owing to their high catalytic activities [25]. Pd(0)/Pd(II) species supported on various materials, such as zeolites, carbons, metal oxides, and polymers, have been successfully used as catalysts for the Heck reaction [26, 27]. However, satisfactory catalytic performance has not been achieved because Pd nanoparticles (Pd NPs) are prone to clustering or aggregation, which results in catalyst deactivation [28–30]. Therefore, it is essential to develop efficient catalytic systems with high performance and recyclability.

Confining metal NPs in porous zeolites [31], carbon nanotubes (CNTs) [32–35], and carbon spheres [36] has been developed as an alternative approach for designing heterogeneous catalysts with enhanced activity and stability. CNTs have been proposed as a novel class of nanoreactors, owing to their well-defined hollow interiors and high aspect ratios. The application of such confined catalysts have used for asymmetric hydrogenation [37], hydrogenation [38], and other reactions [39–41]. However, the exploration of the cavity of CNTs for the Heck reaction has rarely been reported. Therefore, we comparatively studied the Heck reaction under the catalysis of Pd NPs encapsulated within the CNTs and

those attached on the surface of CNTs. The Pd NPs confined in the CNTs (referred to as Pd-in-CNT) showed remarkably better catalytic activity than those on the CNT surface (referred to as Pd-out-CNT) in the coupling of iodobenzene (PhI) and methyl acrylate (MA) to form methyl cinnamate.

2 Results and Discussion

BET analyses were conducted to investigate the porosity of the samples (different treatment procedures for CNT-in and CNT-out are detailed listed in Figure S1). The values of the BET surface area, average pore volume, and pore size are listed in Table 1. The BET specific surface area, average pore volume, and pore size of the CNT-in sample are $140 \text{ m}^2 \text{ g}^{-1}$, 0.32 cc g^{-1} , and 8.9 nm , respectively, and those of CNT-out are $94 \text{ m}^2 \text{ g}^{-1}$, 0.22 cc g^{-1} , and 9.2 nm , respectively (Table 1, entries 1 and 2). The small differences in the specific surface areas and pore sizes of the two catalysts are presumably due to the acid treatment (SI, experimental section-1.1). High-resolution transmission electron microscopy (HRTEM) revealed that vigorous treatment conditions caused the CNT ends to open (Figure S2a), while moderate treatment conditions left the caps intact (Figure S2b). Upon loading the Pd species, the surface area of the CNTs decreased to 84 and $67 \text{ m}^2 \text{ g}^{-1}$ for Pd-in-CNT and Pd-out-CNT, respectively (Table 1, entries 3 and 4). This result indicates that the CNT surface was partially shielded by the Pd species. Furthermore, some of the nanotube tips were possibly entirely or partially blocked by the Pd species. Based on inductively coupled plasma–atomic emission spectrometry (ICP-AES), the amounts of Pd loaded in Pd-in-CNT and Pd-out-CNT catalysts were determined to be 4.7 and 4.9 wt%, respectively. According to the chemical adsorption of Pd-CNT catalysts, the Pd dispersion in Pd-in-CNT and Pd-out-CNT is 23.9 and 12.7%, respectively. The bulk crystal structures of the fresh and reacted Pd-CNT catalysts were examined by X-ray diffraction (XRD). Figure 1 shows the XRD patterns of the Pd-in-CNT and Pd-out-CNT catalysts. The diffraction patterns have five broad peaks at

Table 1 Properties of different samples

Entry	Sample	Surface area (m^2/g) ^a	Average pore volume (cc/g)	Pore size (nm)	Pd dispersion (%) ^b	Pd loading (wt%) ^c
1	CNT-in	140	0.32	9.0	–	–
2	CNT-out	94	0.22	9.2	–	–
3	Pd-in-CNT	85	0.28	13.3	23.9	4.7
4	Pd-out-CNT	67	0.20	11.7	12.7	4.9

^aDetermined by N_2 adsorption/desorption using the Brunauer–Emmett–Teller (BET) method and Barrett–Joyner–Halenda (BJH) method

^bDetermined by chemical adsorption

^cDetermined by inductively coupled plasma–atomic emission spectrometry (ICP-AES)

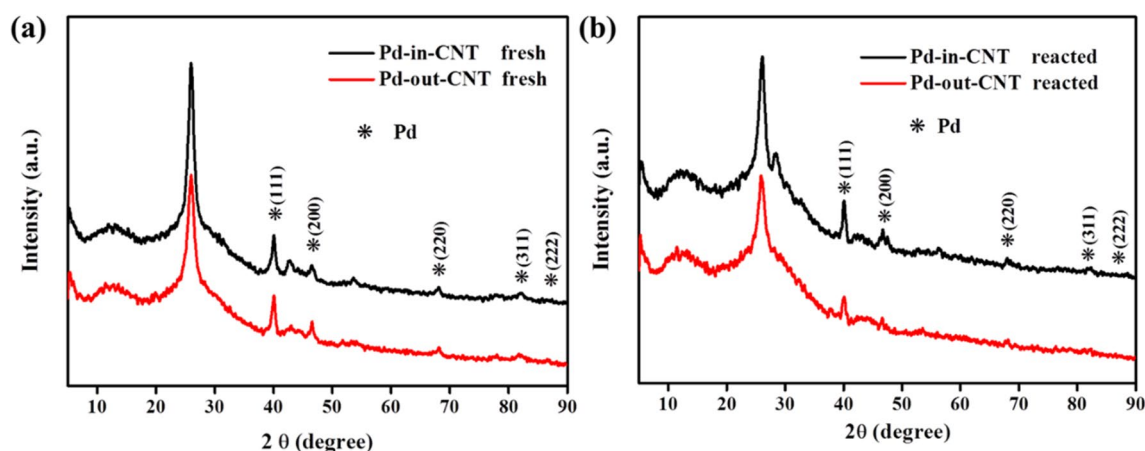


Fig. 1 XRD patterns of fresh catalysts (a) and reacted catalysts (b)

40.1°, 46.7°, 68.1°, 82.1°, and 86.6°, corresponding to the (111), (200), (220), (311), and (222) planes of Pd (JCPDS: 89-4897), respectively. After the reaction, the diffraction peaks of the Pd-out-CNT catalyst weakened (Fig. 1b), indicating an increase in the size of Pd NPs.

HRTEM was used to characterize the Pd-in-CNT and Pd-out-CNT catalysts (Figs. 2 and S3). Figure 2a shows a typical low-magnification TEM image of Pd-in-CNT, in which a portion of Pd NPs is found to be located in the CNT cavity. More than 90% of the Pd NPs are ellipsoidal, as shown in the enlarged TEM image in Fig. 2b. The HRTEM images

of Pd-out-CNT (Fig. 2d and e) show that the Pd NPs on the sample have a face-centered cubic (fcc) Pd lattice, with a Pd(111) interlayer spacing of 0.213 nm. These results indicate that the Pd NPs were loaded externally onto the CNTs with capped ends, as shown in Fig. 2e. Furthermore, for Pd-in-CNT, the particle count taken from many such images (obtained from different regions of the sample) confirmed that more than 80% of the NPs have an average size of 6.0 nm. The particle size distribution of Pd-out-CNT was obtained by the same statistical method based on HRTEM examination (Fig. 2f). The result indicates that the Pd NPs

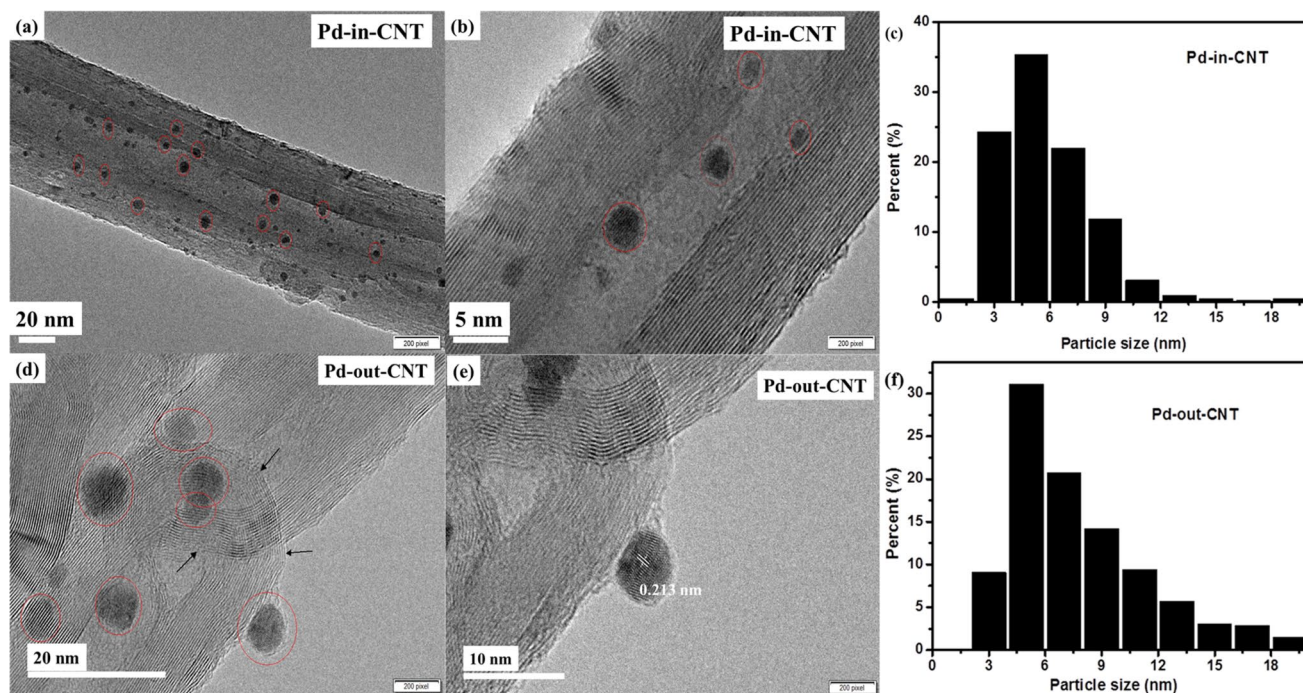


Fig. 2 HRTEM images of Pd-in-CNT (a, b) and Pd-out-CNT (d, e); particle size distribution of Pd NPs, as measured from 500 NPs (c, f)

located on the external wall of the CNT-out are much larger, with an average size of 8.2 nm. This result demonstrates the significance of confining CNTs in a limited space such as a cavity.

Previous studies have revealed that metal oxides located on the internal surface tend to remain in a more reduced state than those dispersed on the external surface [40]. The surface properties of the catalysts were analyzed by X-ray photoelectron spectroscopy (XPS; see Fig. 3a and b). The binding energy of $\text{Pd}^0 3d^{5/2}$ in the Pd-in-CNT catalyst (335.9 eV) is the same as that in the Pd-out-CNT catalyst (335.8 eV). Interestingly, the surface concentration of $\text{Pd}^0 3d$ in the Pd-in-CNT sample (70.8%) is higher than that of the Pd-out-CNT sample (65.4%), suggesting that the CNT channels could hinder the oxidation of surface Pd NPs, which is consistent with the observation made in previous works, indicating that the confined CNT environment is beneficial for maintaining the metal in a lower valence state [42]. The Raman spectra of the two catalysts excited with a 514.5 nm laser line are shown in Fig. 3c and d. The two catalysts exhibit three characteristic peaks at 1341, 1576,

and 1613 cm^{-1} . The first two main bands correspond to the D and G bands of the CNTs. The D band in the Raman spectra of the Pd-in-CNT and Pd-out-CNT is induced by the disorder in the double-resonance process, while the G band is related to the graphite tangential E2g Raman active mode. Therefore, the intensity ratio of the D to G band (I_D/I_G) is commonly used to qualitatively determine the defect content of CNTs, which provides information about the crystallinity of CNTs. For the Pd-in-CNT and Pd-out-CNT samples, the I_D/I_G ratios are 0.76 and 1.07, respectively. This result demonstrates the presence of a small number of structural defects in the graphitic structure of CNTs. The higher the I_D/I_G ratio of the Pd-out-CNT could be due to the formation of new defects after the Pd NPs were attached to the external surface of CNTs.

To verify the confinement effect of CNTs on the catalytic activity of Pd NPs, the Heck reaction between iodobenzene (PhI) and methyl acrylate (MA) was used to evaluate the catalytic performances of the Pd-in-CNT and Pd-out-CNT catalysts (SI, Table S1). The catalytic activities of Pd-in-CNT (red line) and Pd-out-CNT (black line) are presented in

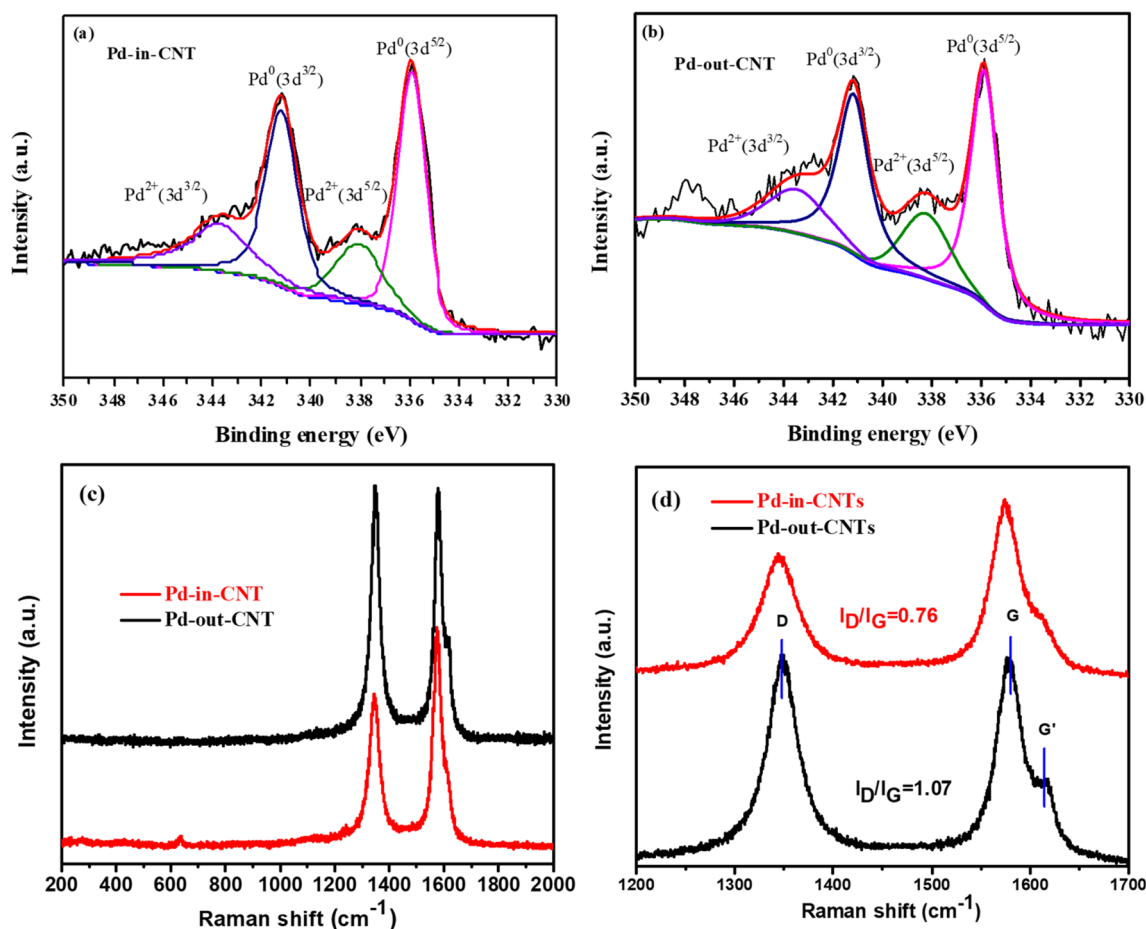


Fig. 3 Structural properties of Pd-in-CNT (a) and Pd-out-CNT (b) samples. Pd 3d XPS profiles of the two samples. c, d Raman spectra (the spectra are normalized to the G band intensity)

Fig. 4. The reaction was performed at the atmospheric pressure with 0.1 mol% Pd (10 mg catalyst) in 10 mL of DMF containing iodobenzene (5 mmol) and MA (7.5 mmol). As shown, the Pd-in-CNT catalyst provides high catalytic efficiency at different temperatures. In the presence of Pd-in-CNT and Pd-out-CNT catalysts, the conversion of the Heck reaction reached 99% at 100 °C within 30 and 90 min, respectively. In the presence of Pd-in-CNT, the reaction rate of iodobenzene reached up to $0.816 \text{ mol L}^{-1} \text{ h}^{-1}$ within 20 min at 100 °C, surpassing that of the Pd-out-CNT catalyst (reaction rate: $0.087 \text{ mol L}^{-1} \text{ h}^{-1}$). This result indicates that the CNT-confined Pd catalyst has 9.4 times higher activity than the Pd NPs located on the external walls of the CNTs in the Heck reaction. Considering the internal and external diffusion of the two samples, although the Pd nanoparticles in Pd-out-CNT are much more accessible to the reaction substrate, the Pd-in-CNT catalyst shows higher performance. A possible explanation for this difference in activity is that

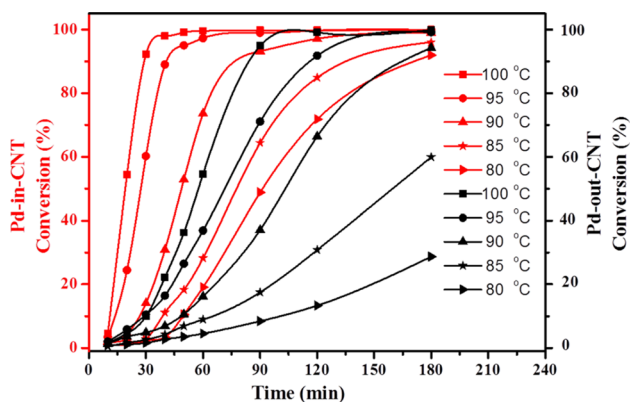


Fig. 4 Variation in the performance of Pd-in-CNT and Pd-out-CNT catalysts in the Heck reaction between iodobenzene and methyl acrylate with the temperature

the oxidative addition of aryl iodide is faster with Pd-in-CNT than with Pd-out-CNT [22]. This is possibly because of the smaller particle size and modified redox properties of the Pd-in-CNT catalyst. According to HRTEM results, Pd NPs in Pd-in-CNT are smaller (6.0 nm, Fig. 2c) than those in Pd-out-CNT (8.2 nm, Fig. 2f). After 20 min of the reaction at 100 °C, the conversion of iodobenzene on Pd-in-CNT reached 53%, while the reaction product could hardly be detected for Pd-out-CNT at the same reaction temperature. Changing the reaction temperature to 80 °C led to decreased conversion, especially with the Pd-out-CNT catalyst. Furthermore, the conversion with the Pd-out-CNT catalyst improved within 90 min from 10 to 95% upon increasing the reaction temperature from 80 to 100 °C. The catalytic activity of the Pd-in-CNT sample at 90 °C is equivalent to that observed at 100 °C with the Pd-out-CNT catalyst, implying a superior performance of the former. These comparisons demonstrate that the confinement effect of CNTs facilitates the reducibility of Pd-in-CNT catalyst, thus leading to the excellent catalytic activity of Pd-in-CNT in the Heck reaction. Hence, the Pd-in-CNT catalyst shows a higher catalytic performance than the Pd-out-CNT catalyst at all reaction temperatures.

To explore the confinement effect of these catalysts, the reducibility of Pd-in-CNT and Pd-out-CNT catalysts was investigated by H_2 temperature-programmed reduction (H_2 -TPR) and CO-microcalorimetric adsorption. In the H_2 -TPR analysis, Pd precursors are converted first to PdO and then to metallic Pd under H_2 ambient with increasing temperature. The key temperatures of the phase transformations are noted in Fig. 5a. The phase transformation in the presence of Pd-in-CNT at each reduction step occurs at a lower temperature than that in the presence of Pd-out-CNT. For example, the reduction of $(\text{NH}_4)_2\text{PdCl}_6$ to PdO begins at 126 °C for Pd-in-CNT, which is ~ 12 °C lower than that

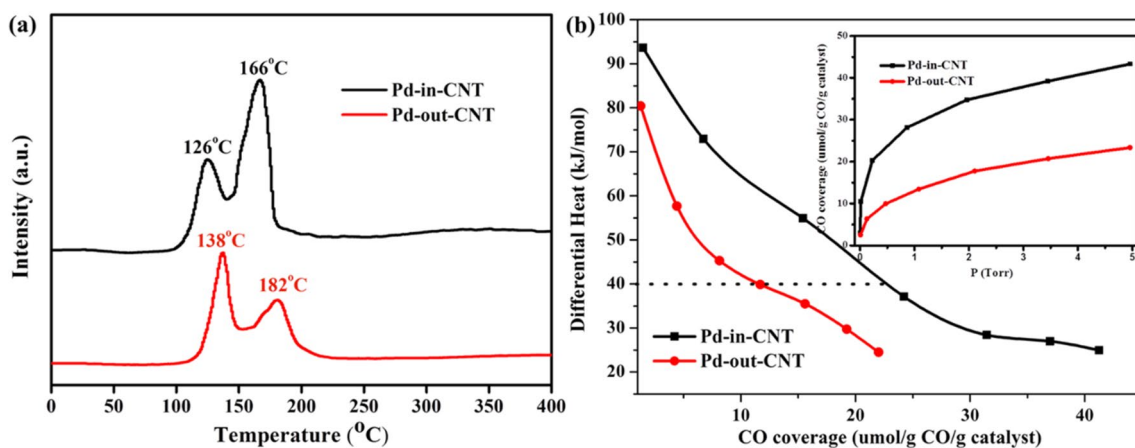


Fig. 5 **a** H_2 temperature-programmed reduction profiles of Pd-in-CNT and Pd-out-CNT (theoretical Pd loading: 5 wt%) catalysts. **b** Differential heat versus coverage for CO adsorption on the two catalysts at 40 °C

for the Pd-out-CNT catalyst during H_2 -TPR. The reduction temperatures of PdO to Pd are 166 and 182 °C under the catalysis of Pd-in-CNT and Pd-out-CNT, respectively. CO-microcalorimetric adsorption experiments were performed to investigate the difference in the catalytic activity of the Pd-in-CNT and Pd-out-CNT catalysts. Figure 5b shows the plots of differential heat versus adsorbate (CO) coverage on the two catalysts. The initial differential heats for CO adsorption on the catalysts were in the range of 80–100 kJ mol⁻¹; the value is 94 kJ mol⁻¹ for Pd-in-CNT, greater than that of Pd-out-CNT (80 kJ mol⁻¹), consistent with the trend of the catalyst performance in the Heck reaction involving iodobenzene conversion. Owing to the adsorption on weaker sites and interaction between the adsorbed species, the differential heat of adsorption decreased with the increase in CO coverage, as shown in Fig. 5b. The inset in Fig. 5b shows that Pd-in-CNT contains more sites for CO adsorption (23 $\mu\text{mol g}^{-1}$) than Pd-out-CNT (12 $\mu\text{mol g}^{-1}$). The results indicate that this difference in the strong adsorption sites and

amount of adsorption sites between the two catalysts correlate well with their activity in the Heck reaction (Fig. 4), suggesting that the strong adsorption sites of the catalysts are responsible for the Heck reaction (oxidative addition of the substrate and reductive elimination of the intermediate). The strength of CO adsorption can be correlated with the electron cloud density of the Pd NPs in these catalysts. Hence, the confinement of Pd NPs inside CNTs affects their catalytic performance in the Heck reaction.

To demonstrate the scope of the confinement effect and stability of Pd-in-CNT and Pd-out-CNT catalysts in the Heck reaction involving aryl iodide and MA, various aryl iodides were coupled with MA at 100 °C under the reaction conditions shown in Fig. 6a–f. The results indicated that Pd-in-CNT has higher activity than Pd-out-CNT in the Heck reaction of most substrates, except for 4-iodobenzonitrile. The aryl iodides with electron-withdrawing groups (-F, -Cl, and -Br) at the para position reacted smoothly with MA and provided high yields. Moreover, the stronger the

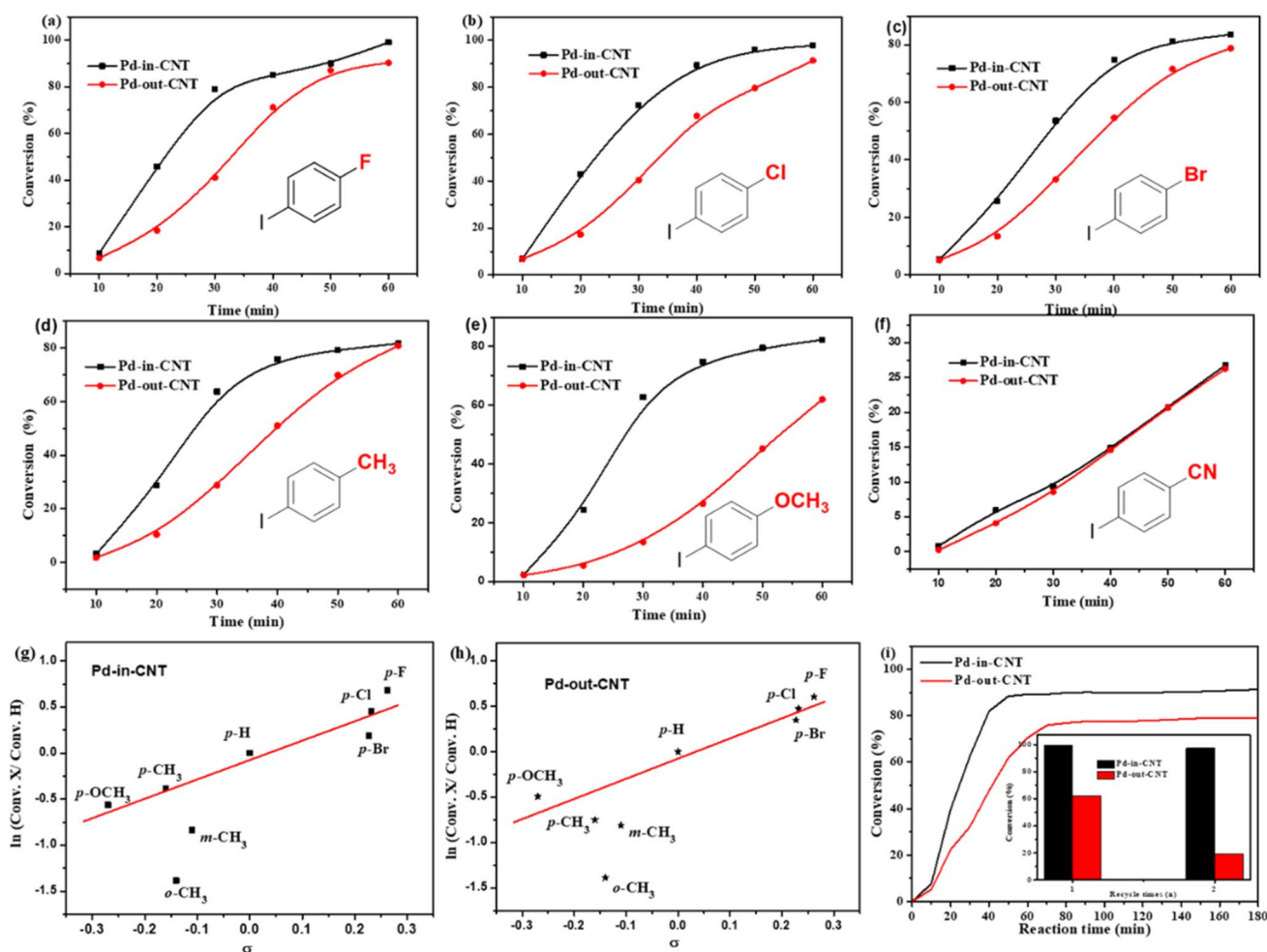


Fig. 6 Reaction scope of aryl iodides and methyl acrylate (a–f). Hammett plot for the rate constants of a series of *p*-substituted iodobenzene (g, h). i Thermal filtration experiments of Pd-in-CNT and Pd-out-CNT catalysts

electron-withdrawing group ($-F > -Cl > -Br$), the higher the yield of the reaction (Fig. 6a–c). In contrast, the electron-withdrawing substituent ($-CN$) leads to an abnormal result (Fig. 6f), which requires further study. MA reacted with electron-donating groups ($-CH_3$ and $-OCH_3$) at the para position relative to iodine aryl, and led to an evident decrease in the aryl iodide conversion (Fig. 6d, e). To further investigate the reaction mechanism, the Hammett plot for the rate constants of a series of *p*-substituted iodobenzene derivatives ($X = p\text{-OMe}$, *p*-Me, *m*-Me, *o*-Me, *p*-H, *p*-Br, *p*-Cl, and *p*-F) was obtained. A linear relationship between $\ln(\text{Conv. X}/\text{Conv. H})$ and Brown–Okamoto constant σ was observed (Fig. 6g, h), suggesting that the Heck reaction is sensitive to the substituent. The electron-withdrawing groups ($-F$, $-Cl$, and $-Br$) weaken the C–I bond, thus favoring a rapid reaction of the substituted iodobenzene and MA. However, the electron-donor substituents (*p*-OMe, *m*-Me, *o*-Me, and *p*-Me) disfavor the electrophilic reaction, leading to unsatisfactory results. Unusual results were obtained with iodobenzene substituted with methyl groups at the meta, ortho, and para positions, probably because of the steric hindrance. To investigate the reusability and stability of the two catalysts during the reaction, thermal filtration and recyclability experiments were performed. Iodobenzene was reacted with MA at 100 °C. The catalysts were removed after performing the reaction for 40 min, and the reaction was then continued with the reaction liquid. The heat filtration diagram shows that the conversion rate in the presence of the two catalysts increases to some extent when the reaction was extended beyond 40 min (the conversion on Pd-in-CNT increases from 83 to 88%, while that on Pd-out-CNT increases from 48 to 75% between 40 and 60 min), indicating that a certain amount of the Pd NPs of the catalysts dissolved to form molecular Pd in the solution [43–45]. However, the amount of Pd leached from the Pd-in-CNT is much lower than that leached from the Pd-out-CNT catalyst. Furthermore, after washing with DMF, the Pd-in-CNT showed no evident decay in the activity in the Heck reaction in the second cycle (Fig. 6i). In contrast, the activity of the Pd-out-CNT catalyst decreased dramatically. These results indicate that the confinement of Pd within CNTs can also affect their stability in the Heck reaction.

3 Conclusion

Pd nanoparticles (NPs) were selectively loaded both inside and outside the multiwalled CNTs through a simple impregnation method, and were used for catalyzing the Heck reaction. These catalysts exhibited remarkable performance in the Heck reaction with iodobenzene and methyl acrylate. The overall reaction rate of iodobenzene ($0.816 \text{ mol L}^{-1} \text{ h}^{-1}$) on Pd-in-CNT exceeds that achieved on Pd-out-CNT

($0.087 \text{ mol L}^{-1} \text{ h}^{-1}$), although the latter is much more accessible to the reaction substrate. The activity of the Pd-in-CNT catalyst is 9.4 times higher than that of the Pd-out-catalyst in the Heck reaction. These catalysts can also be used for Heck reactions with different substrates. The cavity of CNTs affords a stable microenvironment for the immobilized Pd active sites. According to the H_2 -TPR, CO-calorimetric adsorption, and TEM results, the higher catalytic performance of Pd-in-CNT may also be attributed to the smaller Pd particle size and modified redox properties.

Supplementary Information The online version contains supplementary material available at <https://doi.org/10.1007/s10562-021-03577-w>.

Acknowledgements This work was supported by the National Natural Science Foundation of China (Nos. 21908183 and 21506714) and Key Laboratory of Basic Chemistry, the State Ethnic Affairs Commission (2020PTJS20002). We greatly appreciate Prof. Lin Li (Dalian Institute of Chemical Physics, Chinese Academy of Sciences) for his help with the microcalorimetric measurements. We would like to thank Editage (www.editage.cn) for English language editing.


References

1. Astruc D (2020) Introduction: nanoparticles in catalysis. *Chem Rev* 120:461–463
2. Climent MJ, Corma A, Iborra S (2011) Heterogeneous catalysts for the one-pot synthesis of chemicals and fine chemicals. *Chem Rev* 111:1072–1133
3. Zhang LL, Zhou MX, Wang AQ, Zhang T (2020) Selective hydrogenation over supported metal catalysts: from nanoparticles to single atoms. *Chem Rev* 120:683–733
4. Blanco M, Mosconi D, Tubaro C, Biffis A, Badocco D, Pastore P, Otyepka M, Bakandritsos A, Liu ZB, Ren WC, Agnoli S, Granozzi G (2019) Palladium nanoparticles supported on graphene acid: a stable and eco-friendly bifunctional C–C homo- and cross-coupling catalyst. *Green Chem* 21:5238–5247
5. Favier I, Pla D, Gomez M (2020) Palladium nanoparticles in polyols: synthesis, catalytic couplings, and hydrogenations. *Chem Rev* 120:1146–1183
6. Lercher JA (2015) New Lewis acid catalyzed pathway to carbon-carbon bonds from methanol. *ACS Cent Sci* 1:350–351
7. Lu XJ, Wu JJ, Lin TQ, Wan DY, Huang FQ, Xie XM, Jiang MH (2011) Low-temperature rapid synthesis of high-quality pristine or boron-doped graphene via Wurtz-type reductive coupling reaction. *J Mater Chem* 21:10685–10689
8. Dubey AV, Kumar AV (2020) A bio-inspired magnetically recoverable palladium nanocatalyst for the Ullmann coupling reaction of aryl halides and arylboronic acids in aqueous media. *Appl Organomet Chem* 34:5570
9. Hassan J, Sévignon M, Gozzi C, Schulz E, Lemaire M (2002) Aryl-aryl bond formation one century after the discovery of the Ullmann reaction. *Chem Rev* 102:1359–1469
10. Rodriguez-Fernandez J, Haastrup MJ, Schmidt SB, Gronborg SS, Mammen MHR, Lauritsen JV (2020) Molecular nanowire bonding to epitaxial single-layer MoS_2 by an on-surface Ullmann coupling reaction. *Small* 16:1906892
11. Vucetic N, Virtanen P, Nuri A, Mattsson I, Aho A, Mikkola JP, Salmi T (2019) Preparation and characterization of a new bis-layered supported ionic liquid catalyst (SILCA) with an unprecedented activity in the Heck reaction. *J Catal* 371:35–46

12. Yu R, Liu R, Deng J, Ran MF, Wang N, Chu W, He ZW, Du Z, Jiang CF, Sun WJ (2018) Pd nanoparticles immobilized on carbon nanotubes with a polyaniline coaxial coating for the Heck reaction: coating thickness as the key factor influencing the efficiency and stability of the catalyst. *Catal Sci Technol* 8:1423–1434
13. Zhu KL, Dunne J, Shaver MP, Thomas SP (2017) Iron-catalyzed Heck-type alkenylation of functionalized alkyl bromides. *ACS Catal* 7:2353–2356
14. Phapale VB, Cardenas DJ (2009) Nickel-catalysed Negishi cross-coupling reactions: scope and mechanisms. *Chem Soc Rev* 38:1598–1607
15. Espinet P, Echavarren AM (2004) The mechanisms of the Stille reaction. *Angew Chem Int Ed* 43:4704–4734
16. Chen ZP, Vorobyeva E, Mitchell S, Fako E, Ortuno MA, Lopez N, Collins SM, Midgley PA, Richard S, Vile G, Perez-Ramirez J (2018) A heterogeneous single-atom palladium catalyst surpassing homogeneous systems for Suzuki coupling. *Nat Nanotechnol* 13:702–707
17. Krishnan KK, Saranya S, Rohit KR, Anilkumar G (2019) A novel zinc-catalyzed Suzuki-type cross-coupling reaction of aryl boronic acids with alkynyl bromides. *J Catal* 372:266–271
18. Albinana PA, El Haskouri J, Marcos MD, Estevan F, Amoros P, Ubieda MA, Perez-Pla F (2018) A new efficient, highly dispersed, Pd nanoparticulate silica supported catalyst synthesized from an organometallic precursor. Study of the homogeneous vs. heterogeneous activity in the Suzuki-Miyaura reaction. *J Catal* 367:283–295
19. Platonova YB, Volov AN, Tomilova LG (2019) Palladium(II) octaalkoxy- and octaphenoxypthalocyanines: synthesis and evaluation as catalysts in the Sonogashira reaction. *J Catal* 373:222–227
20. Balanta A, Godard C, Claver C (2011) Pd nanoparticles for C-C coupling reactions. *Chem Soc Rev* 40:4973–4985
21. Eremin DB, Ananikov VP (2017) Understanding active species in catalytic transformations: from molecular catalysis to nanoparticles, leaching, “cocktails” of catalysts and dynamic systems. *Coord Chem Rev* 346:2–19
22. Reetz MT, de Vries JG (2004) Ligand-free Heck reactions using low Pd-loading. *Chem Commun*. <https://doi.org/10.1039/B406719N>
23. Schmidt AF, Al Halaiqa A, Smirnov VV (2006) Interplays between reactions within and without the catalytic cycle of the Heck reaction as a clue to the optimization of the synthetic protocol. *Synlett* 2006:2861–2878
24. Liu LC, Corma A (2018) Metal catalysts for heterogeneous catalysis: from single atoms to nanoclusters and nanoparticles. *Chem Rev* 118:4981–5079
25. Sadjadi S, Lazzara G, Malmir M, Heravi MM (2018) Pd nanoparticles immobilized on the poly-dopamine decorated halloysite nanotubes hybridized with N-doped porous carbon monolayer: a versatile catalyst for promoting Pd catalyzed reactions. *J Catal* 366:245–257
26. Gnad C, Dachwald O, Raudaschl-Sieber G, Köhler K (2019) Synthesis of methyl palladium complexes on silica as single site catalysts activating C-Cl bonds in Heck reactions. *J Catal* 375:257–266
27. Duan H, Li MH, Zhang GH, Gallagher JR, Huang ZL, Sun Y, Luo Z, Chen HZ, Miller JT, Zou RQ, Lei AW, Zhao YL (2015) Single-site palladium(II) catalyst for oxidative Heck reaction: catalytic performance and kinetic investigations. *ACS Catal* 5:3752–3759
28. Huang YB, Gao SY, Liu TF, Lu J, Lin X, Li HF, Cao R (2012) Palladium nanoparticles supported on mixed-linker metal-organic frameworks as highly active catalysts for Heck reactions. *ChemPlusChem* 77:106–112
29. Kunfi A, May Z, Nemeth P, London G (2018) Polydopamine supported palladium nanoparticles: highly efficient catalysts in Suzuki cross-coupling and tandem Suzuki cross-coupling/nitroarene reductions under green reaction conditions. *J Catal* 361:84–93
30. Rangel ER, Maya EM, Sanchez F, de la Campa JG, Iglesias M (2015) Palladium-heterogenized porous polyimide materials as effective and recyclable catalysts for reactions in water. *Green Chem* 17:466–473
31. Wang CT, Zhang J, Qin GQ, Wang L, Zuidema E, Yang Q, Dang SS, Yang CG, Xiao JP, Meng XJ, Mesters C, Xiao FS (2020) Direct conversion of syngas to ethanol within zeolite crystals. *Chem Soc Rev* 6:646–657
32. Chen TW, Li ZQ, Wang K, Wang FB, Xia XH (2018) Exploring the confinement effect of carbon nanotubes on the electrochemical properties of Prussian blue nanoparticles. *Langmuir* 34:6983–6990
33. Ning YX, Wei MM, Yu L, Yang F, Chang R, Liu Z, Fu Q, Bao XH (2015) Nature of interface confinement effect in oxide/metal catalysts. *J Phys Chem C* 119:27556–27561
34. Pan XL, Bao XH (2011) The effects of confinement inside carbon nanotubes on catalysis. *Acc Chem Res* 44:553–562
35. Wang Y, Rong ZM, Wang Y, Zhang P, Wang Y, Qu JP (2015) Ruthenium nanoparticles loaded on multiwalled carbon nanotubes for liquid-phase hydrogenation of fine chemicals: an exploration of confinement effect. *J Catal* 329:95–106
36. Liu XY, Lan GJ, Boyjoo Y, Qian LH, Gu S, Price CAH, Wang L, Li Y, Liu J (2019) N-doped carbon spheres impregnated with highly monodispersed ruthenium nanoparticles as a hydrogenation catalyst. *Chem Eng J* 374:895–903
37. Chen ZJ, Guan ZH, Li MR, Yang QH, Li C (2011) Enhancement of the performance of a platinum nanocatalyst confined within carbon nanotubes for asymmetric hydrogenation. *Angew Chem Int Ed* 50:4913–4917
38. Wang D, Yang GH, Ma QX, Wu MB, Tan YS, Yoneyama Y, Tsubaki N (2012) Confinement effect of carbon nanotubes: copper nanoparticles filled carbon nanotubes for hydrogenation of methyl acetate. *ACS Catal* 2:1958–1966
39. Grommet AB, Feller M, Klajn R (2020) Chemical reactivity under nanoconfinement. *Nat Nanotechnol* 15:256–271
40. Xiao JP, Pan XL, Guo SJ, Ren PJ, Bao XH (2015) Toward fundamentals of confined catalysis in carbon nanotubes. *J Am Chem Soc* 137:477–482
41. Cui TT, Dong JH, Pan XL, Yu T, Fu Q, Bao XH (2019) Enhanced hydrogen evolution reaction over molybdenum carbide nanoparticles confined inside single-walled carbon nanotubes. *J Energy Chem* 28:123–127
42. Chen W, Pan X, Bao X (2007) Tuning of redox properties of iron and iron oxides via encapsulation within carbon nanotubes. *J Am Chem Soc* 129:7421–7426
43. Pröckl SS, Kleist W, Gruber MA, Köhler K (2004) In situ generation of highly active dissolved palladium species from solid catalysts—a concept for the activation of aryl chlorides in the Heck reaction. *Angew Chem Int Ed* 43:1881–1882
44. Gnad C, Abram A, Urstöger A, Weigl F, Schuster M, Köhler K (2020) Leaching mechanism of different palladium surface species in Heck reactions of aryl bromides and chlorides. *ACS Catal* 10:6030–6041
45. Biffis A, Centomo P, Zotto AD, Zecca M (2018) Pd metal catalysts for cross-couplings and related reactions in the 21st century: a critical review. *Chem Rev* 118:2249–2295

Publisher's Note Springer Nature remains neutral with regard to jurisdictional claims in published maps and institutional affiliations.

Authors and Affiliations

Zhengxiu Luo¹ · Deng Xiang¹ · Xiaoyan Pei¹ · Lu Wang² · Zhigang Zhao¹ · Wenjing Sun³ · Maofei Ran¹ · Tao Dai¹ 

¹ College of Chemistry & Environment, Southwest Minzu University, Chengdu 610041, China

² College of Animal & Veterinary Sciences, Southwest Minzu University, Chengdu 610041, China

³ China-America Cancer Research Institute, Key Laboratory for Medical Molecular Diagnostics of Guangdong Province, Guangdong Medical University, Dongguan 523808, Guangdong, China